JACS
JOURNAL OF THE AMERICAN CHEMICAL SOCIETY
Article
pubs.acs.org/JACS

Slow Magnetic Relaxation Induced by a Large Transverse Zero-Field Splitting in a $Mn^{II}Re^{IV}(CN)_2$ Single-Chain Magnet

Xiaowen Feng,[†,∥] Junjie Liu,[‡,∥] T. David Harris,[†] Stephen Hill,*[,§] and Jeffrey R. Long*[,†]

[†]Department of Chemistry, University of California, Berkeley, California 94720, United States

[‡]Department of Physics, University of Florida, Gainesville, Florida 32611, United States

[§]Department of Physics and National High Magnetic Field Laboratory, Florida State University, Tallahassee, Florida 32310, United States

Supporting Information

ABSTRACT: The model compounds $(NBu_4)_2[ReCl_4(CN)_2]$ (**1**), $(DMF)_4ZnReCl_4(CN)_2$ (**2**), and $[(PY5Me_2)_2Mn_2ReCl_4(CN)_2](PF_6)_2$ (**3**) have been synthesized to probe the origin of the magnetic anisotropy barrier in the one-dimensional coordination solid $(DMF)_4MnReCl_4(CN)_2$ (**4**). High-field electron paramagnetic resonance spectroscopy reveals the presence of an easy-plane anisotropy ($D > 0$) with a significant transverse component, E, in compounds **1**−**3**. These findings indicate that the onset of one-dimensional spin correlations within the chain compound **4** leads to a suppression of quantum tunneling of the magnetization within the easy plane, resulting in magnetic bistability and slow relaxation behavior. Within this picture, it is the transverse E term associated with the Re^{IV} centers that determines the easy axis and the anisotropy energy scale associated with the relaxation barrier. The results demonstrate for the first time that slow magnetic relaxation can be achieved through optimization of the transverse anisotropy associated with magnetic ions that possess easy-plane anisotropy, thus providing a new direction in the design of single-molecule and single-chain magnets.

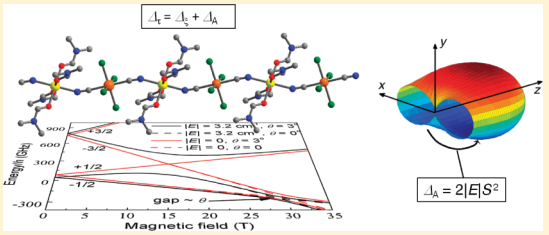

INTRODUCTION

Molecules that exhibit slow magnetic relaxation upon removal from a polarizing magnetic field, referred to as single-molecule magnets,[1] have received considerable attention owing to their potential utility in applications such as spin-based information storage.[2] In these systems, the slow relaxation arises from the action of a uniaxial magnetic anisotropy, quantified by the axial zero-field splitting parameter, D, on a high-spin ground state, S. This phenomenon engenders a magnetic anisotropy energy barrier, Δ_A, with respect to reversal of the spin of the molecule, where $\Delta_A = S^2|D|$ for integer S and $(S^2 - {}^1/_4)|D|$ for half-integer S. For practical applications of single-molecule magnets to be fully realized, the relaxation barrier must be large enough to ensure stability of the moment orientation to thermal and quantum fluctuations.

Analogous relaxation behavior has been observed more recently in one-dimensional coordination compounds, known as single-chain magnets,[3,4] which consist of paramagnetic ions linked together via bridging ligands. Considering the pursuit of high relaxation barriers in low-dimensional paramagnets, single-chain magnets possess a distinct advantage over single-molecule magnets. The advantage stems from the exchange coupling (J) between the magnetic ions, which adds an additional energy term known as the correlation energy, Δ_ξ, to the expression for the relaxation barrier. Assuming a $-2JS_1 \cdot S_2$ interaction between neighboring spin units, the magnitude of the correlation energy for a chain is $\Delta_\xi = 4|J|S^2$ in the Ising limit, where $|D/J| > 4/3$, while $\Delta_\xi = 4S^2\,(|JD|)^{1/2}$ in the Heisenberg limit, where $|D| \ll |J|$.[3g,j] The total energy barrier with respect to spin reversal can then be expressed as $\Delta_\tau = \Delta_A + 2\Delta_\xi$ for an infinite chain in which the nucleation of reversed spins necessarily requires the creation of two propagating domain walls.[3g,5,6] In contrast, nucleation from the ends of finite-length chains gives rise to an expression for the total energy of $\Delta_\tau = \Delta_A + \Delta_\xi$. At low temperatures, the relaxation dynamics of single-chain magnets typically fall into the latter category, where the finite chain lengths are caused by crystalline defects.

A negative D value assures that states with maximum spin projection ($M_S = \pm S$) along the z axis lie lowest in energy while intermediate spin projections lie higher in energy, such that a classical rotation of the moment from $M_S = +S$ to $-S$ requires excitation over an energy barrier. In the absence of quantum tunneling, which is typically weak for large values of S, it is this anisotropy that gives rise to a magnetically bistable ground state. In contrast, a positive D value and magnetic bistability are widely regarded as being antagonistic, as the ground state in this situation (a singlet for integer S and a Kramers doublet for half-integer S) has minimal spin projection onto the z axis. Moreover, for the purely axial case, the spin has no preferred orientation within the easy (xy) plane. Even in cases involving appreciable transverse (xy) anisotropy, $E(S_x^2 - S_y^2)$, quantum tunneling, which is severe for states that are close in energy, prevents localization of the spin along a preferred direction

Received: February 9, 2012
Published: April 11, 2012

   dx.doi.org/10.1021/ja301338d | J. Am. Chem. Soc. 2012, 134, 7521−7529

within the easy plane. In this context, it is not surprising that it is a commonly held principle that negative D values are essential in the design of single-molecule and single-chain magnets.[7,8]

As noted above, quantum tunneling prevents localization of a magnetic moment along a preferred axis in the case of a quantum spin subjected to easy-plane anisotropy, a simple manifestation of the fact that S_x and S_y do not commute with S_z. However, the situation is quite different in the classical limit, where the magnetic moment associated with a macroscopic easy-plane system may have a preferred (easy) axis when any transverse anisotropy of the form $E(S_x^2 - S_y^2)$ is factored in. In this scenario, the easy-axis would lie along either the x or y direction, depending on the sign of E, and a highly anisotropic energy barrier would prevent rotation of the moment from $+x$ to $-x$ (or $+y$ to $-y$). Furthermore, the maximum barrier height, corresponding to rotation of the moment through z, would be dictated by D, while the barrier height corresponding to rotation within the xy plane would be dictated instead by E. Such a scenario has, so far, not been considered as a possible source of slow magnetic relaxation behavior in either single-molecule or single-chain magnets.

Recently, we reported the synthesis of the series of cyano-bridged single-chain magnets $(DMF)_4MReCl_4(CN)_2$ (M = Mn, Fe, Co, Ni), assembled from the building unit $[ReCl_4(CN)_2]^{2-}$.[4] Magnetic analyses revealed that these chain compounds lie in neither the Ising nor Heisenberg limits, which complicates the comparison of the observed Δ_τ values with those calculated via the experimentally determined J and D values. Given that the magnetic behavior of the compounds results from a combination of the magnetic anisotropy of the individual spin centers and the interactions between adjacent spin centers, the study of molecules mimicking small fragments of the chain may afford insight into the mechanisms leading to slow magnetic relaxation.

Herein, we report detailed high-frequency, high-field electron paramagnetic resonance (EPR) studies of three compounds, $(Bu_4N)_2[trans\text{-}ReCl_4(CN)_2]\cdot 2DMA$ (**1**), $(DMF)_4ZnReCl_4(CN)_2$ (**2**), and $[(PY5Me_2Mn)_2ReCl_4(CN)_2](PF_6)_2$ (**3**; $PY5Me_2$ = 2,6-bis(1,1-bis(2-pyridyl)ethyl)pyridine), elucidating the influence of the metal coordination environment and magnetic interactions on D, to study the magnetic anisotropy of the chain compound $(DMF)_4MnReCl_4(CN)_2$ (**4**). Surprisingly, **1**−**3** exhibit significant biaxiality, with positive D values and a large E, suggesting similar properties in compound **4**. We also describe a mechanism for slow magnetic relaxation in a single-chain magnet that arises due to a barrier created by the transverse anisotropy E rather than the axial anisotropy D. To the best of our knowledge, this is the first observation of slow relaxation arising from E in any coordination compound.

EXPERIMENTAL SECTION

Preparation of Compounds. The compounds $[(PY5Me_2)Mn(CH_3CN)](PF_6)_2$, $(Bu_4N)_2[trans\text{-}ReCl_4(CN)_2]\cdot 2DMA$ (**1**), and $(DMF)_4MnReCl_4(CN)_2$ (**4**) were synthesized as described previously.[1e,4] Solid $(Bu_4N)CN$ was dried in vacuo ($P < 10^{-3}$ Torr) for 36 h using a trap containing P_2O_5 prior to use. All other reagents were obtained from commercial sources and used without further purification. *Caution: Although we have experienced no problems while working with them, perchlorate salts are potentially explosive and should be handled with extreme care and only in small quantities!*

$(DMF)_4ZnReCl_4(CN)_2$ (2). A solution of $Zn(BF_4)_2\cdot H_2O$ (0.014 g, 0.078 mmol) in 2 mL of DMF was added to a solution of **1** (0.030 g, 0.035 mmol) in 2 mL of DMF. The resulting light green solution was allowed to stand for 2 h to afford green plate-shaped crystals suitable for X-ray analysis. The crystals were collected by filtration, washed with successive aliquots of DMF (3 × 1 mL) and Et_2O (3 × 5 mL), and dried in air to afford 0.018 g (70%) of product as a light green solid. IR (neat): ν_{CN} 2170 cm^{-1}. Anal. Calcd for $C_{14}H_{28}Cl_4N_6O_4ReZn$: C, 22.80; H, 1.91; N, 11.40. Found: C, 22.90; H, 1.88; N, 11.32.

$[(PY5Me_2Mn)_2ReCl_4(CN)_2](PF_6)_2$ (3). A solution of $[(PY5Me_2)Mn(CH_3CN)](PF_6)_2$ (0.035 g, 0.052 mmol) in 2 mL of acetonitrile to a solution of **1** (0.020 g, 0.023 mmol) in 2 mL of acetonitrile. The resulting bright yellow solution was filtered through diatomaceous earth. Diffusion of diethyl ether vapor into the filtrate afforded yellow blade-shaped crystals suitable for X-ray analysis. The crystals were collected by filtration, washed with successive aliquots of Et_2O (3 × 5 mL), and dried in air to give 0.022 g (62%) of product as a light green solid. IR (neat): ν_{CN} 2156 cm^{-1}. Anal. Calcd for $C_{56}H_{50}Cl_4F_{12}Mn_2N_{12}P_2Re$: C, 41.54; H, 3.11; N, 10.38. Found: C, 41.27; H, 3.65; N, 10.88.

X-ray Structure Determinations. Single crystals of compounds **2** and **3** were coated with Paratone-N oil and mounted on glass fibers or Kaptan loops. The crystals were then quickly transferred to a Bruker MICROSTAR diffractometer and cooled in a stream of nitrogen gas. Preliminary cell data were collected, giving unit cells with a triclinic or monoclinic Laue group, as established using the SMART[9] or APEX2[10] program package. The unit cell parameters were later refined against all data. A full hemisphere of data were collected for all compounds. None of the crystals showed significant decay during data collection. Data were integrated and corrected for Lorentz and polarization effects using SAINT[11] and were corrected for absorption effects using SADABS.[12]

Space group assignments were based upon systematic absences, E statistics, and successful refinement of the structures. Structures were solved by direct methods and expanded through successive difference Fourier maps. They were refined against all data using the SHELXTL[13] program. Thermal parameters for all non-hydrogen atoms were refined anisotropically in all compounds. Table S1 (Supporting Information) summarizes the unit cell and structure refinement parameters for compounds **2** and **3**.

Magnetic Susceptibility Measurements. Magnetic data were collected on a Quantum Design MPMS-XL SQUID magnetometer. Dc susceptibility measurements for **2** were obtained for a microcrystalline powder restrained in its frozen mother liquor within a sealed fused silica tube to prevent sample decomposition. Measurements for compound **3** were performed on microcrystalline powders restrained in a frozen polyethylene bag. All data were corrected for diamagnetic contributions from the sample holder, as well as for the core diamagnetism of each sample (estimated using Pascal's constants).

Electron Paramagnetic Resonance. Single-crystal high-field EPR measurements were carried out in a 35 T resistive magnet. A millimeter vector network analyzer and several different multipliers were used as a microwave source and detector. Powder EPR data were collected in a transmission-type spectrometer based on a 17 T superconducting magnet. A phase-locked Virginia Diodes solid-state source, followed by a cascade of multipliers and amplifiers, was employed as the microwave source.

Other Physical Measurements. Infrared spectra were obtained on a Nicolet Avatar 360 FTIR with an attenuated total reflectance (ATR) accessory. Carbon, hydrogen, and nitrogen analyses were obtained from the Microanalytical Laboratory of the University of California, Berkeley. X-ray powder diffraction data were collected using Cu Kα (λ = 1.5406 Å) radiation on a Siemens D5000 diffractometer.

RESULTS AND DISCUSSION

Synthesis and Structures. Compounds **1**−**3** were synthesized to help understand the magnetic anisotropy of chain compound **4**. Here, **1** contains the $[ReCl_4(CN)_2]^{2-}$ fragment of **4**, while **2** is isostructural to **4** with S = 0 Zn^{II} centers replacing the $S = {}^5/_2$ Mn^{II} centers in the chain. Lastly,

the trinuclear cyano-bridged complex of **3** represents an excised fragment of **4**, where the chain is terminated on each end by the pentadentate capping ligand $PY5Me_2$.

The new compounds **2** and **3** were synthesized through direct combination of $[ReCl_4(CN)_2]^{2-}$ and either $[Zn(DMF)_6]^{2+}$ in DMF for **2** or $[(PY5Me_2)Mn]^{2+}$ in MeCN for **3** (see Figure 1). The crystal structures of **1**–**4** reveal an

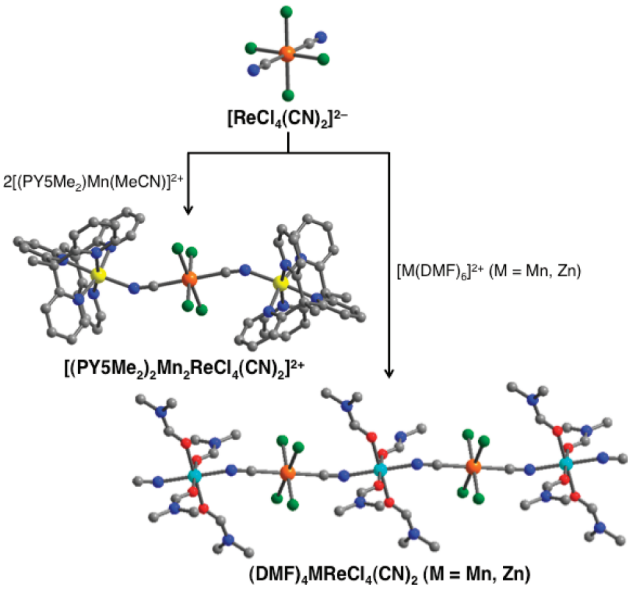

Figure 1. Reaction of *trans*-$[ReCl_4(CN)_2]^{2-}$ (upper) with $[(PY5Me_2)Mn(CH_3CN)]^{2+}$ to form the trinuclear cyano-bridged complex $[(PY5Me_2Mn)_2ReCl_4(CN)_2]^{2+}$ (middle), and with $[M(DMF)_6]^{2+}$ (M = Mn, Zn) to form the one-dimensional solids $(DMF)_4MReCl_4(CN)_2$ (M = Mn, Zn) (lower). Orange, yellow, cyan, green, red, blue, and gray spheres represent Re, Mn, Zn, Cl, O, N, and C atoms, respectively; H atoms have been omitted for clarity.

octahedral coordination geometry at the Re^{IV} center, with four chloride ligands in the equatorial positions and two axial cyanide ligands (see Figures 1 and S1 and S2, Supporting Information). In all structures, the C–Re–Cl and Cl–Re–Cl bond angles are close to 90° (see Table 1). The mean Re–C distances are slightly shorter in the multinuclear species (2.123(6) Å for **2**, 2.134(5) Å for **3**, and 2.125(1) Å for **4**) than the separation of 2.148(4) Å in the molecular salt **1**. Likewise, the mean Re–Cl distances are also longest in **1**, at 2.346(1) Å, compared to 2.313(4) Å in **2**, 2.330(1) Å in **3**, and 2.341(1) Å in **4**. The Re–C–N angles are all close to 180°, while the M–N–C angles (M = Zn, Mn) in **2**–**4** deviate significantly from linearity, being 158.7(1)° in **2**, 154.1(1)° in **3**, and 158.8(1)° in **4**. Such deviations are often observed for M^{II} centers coordinated at the nitrogen end of cyanide and likely arise due to crystal packing forces.[3k,4]

Close comparison of the structures of **1**–**3** with that of **4** were necessary to evaluate the viability of **1**–**3** as models for the chain compound **4**. Inspection of the Re^{IV} coordination spheres in each structure reveals that the local coordination environment of the Re^{IV} ion is essentially constant for all compounds, providing evidence that **1**–**3** are indeed suitable models of **4**. Additionally, within each structure, no significant hydrogen-bonding contacts between chains or molecules are evident in any of the structures, ruling out the presence of any significant pathways for long-range magnetic interactions not present in **4**.

EPR Spectroscopy of 1. Previous fits to variable-temperature dc magnetic susceptibility and magnetization data for **1** suggested significant easy-axis anisotropy with $D = -14.4$ cm^{-1}.[4] However, extracting the sign of D from magnetic data can often be unreliable. Consequently, to obtain a definitive determination of the magnetic anisotropy of the $[ReCl_4(CN)_2]^{2-}$ building block **1**, single-crystal, high-field EPR measurements were performed; experimental details can be found elsewhere.[14] The EPR data can be described by the following effective spin Hamiltonian:

$$\hat{H} = D\hat{S}_z^2 + E(\hat{S}_x^2 - \hat{S}_y^2) + \mu_B \mathbf{B}\cdot\vec{g}\cdot\hat{S} \quad (1)$$

with $S = {}^3/_2$ ($5d^3$, with $S = {}^3/_2$ and $L = 0$) and $0 < |E| < |D|/3$. Figure 2 plots the peak positions of EPR transitions observed via high-field studies at 1.3 K (see also Figure S3, Supporting Information). In this experiment, the crystal was oriented so that the field was aligned close to one of the principal axes of the magnetoanisotropy tensor, determined to be the magnetic hard (z) axis (see below). The most notable feature of these low-temperature spectra is the fact that three resonances are observed in the frequency range from 60 to 130 GHz (see Figure 2, inset). The sharp peak at low field, marked by a blue arrow, corresponds to a transition within the lowest Kramers doublet, while the broad peaks at high field, marked by red arrows, correspond to inter-Kramers transitions. The differences in line width can be explained on the basis of D and E strains, which primarily influence inter-Kramers transitions.[15] Variable-temperature studies at 126.9 GHz (see Figure S4, Supporting Information) indicate that all three resonances correspond to excitations from the lowest lying energy level within the $S = {}^3/_2$ manifold.

Two possible scenarios, both involving significant biaxiality where an E term approaches $|D|/3$, could account for the high-

Table 1. Selected Mean Interatomic Distances (Å) and Angles (deg) for $(Bu_4N)_2[trans\text{-}ReCl_4(CN)_2]\cdot 2DMA$ (1), $(DMF)_4ZnReCl_4(CN)_2$ (2), $[(PY5Me_2Mn)_2ReCl_4(CN)_2](PF_6)_2$ (3), and $(DMF)_4MnReCl_4(CN)_2$ (4)

	1	2	3	4
Re–Cl	2.351(1), 2.341(1)	2.312(4), 2.316(3)	2.344(2), 2.330(1)	2.340(1), 2.343(2)
Re–C	2.148(4)	2.123(6)	2.134(5)	2.125(1)
M–N		2.121(2)	2.192(1)	2.228(1)
M–Npy			2.224(4)	
M–O		2.100(2)		2.181(1)
Re–C–N	177.2(1)	175.0(1)	175.2(1)	175.8(1)
M–N–C		158.8(1)	154.1(1)	158.8(1)
Cl–Re–Cl	90.1 (4)	90.5(1)	90.1(4)	90.6(1)
C–Re–Cl	88.5(1), 89.5(1)	88.1(2), 89.2(1)	89.0(4), 89.6(1)	89.0(1), 88.9(1)

dx.doi.org/10.1021/ja301338d | J. Am. Chem. Soc. 2012, 134, 7521–7529

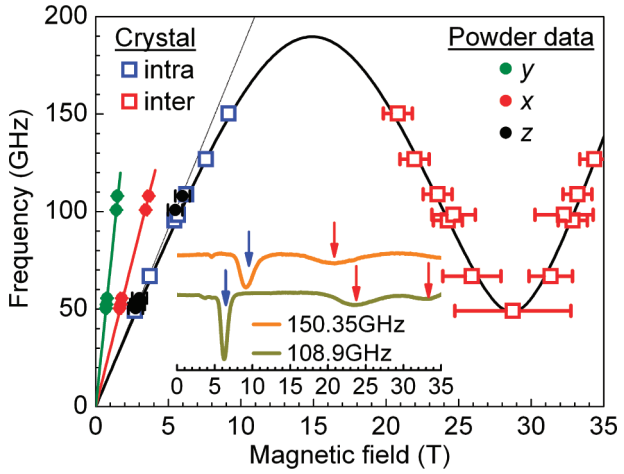

Figure 2. Main panel: EPR peak positions observed for a single crystal of **1** at 1.3 K with the field aligned 3° away from the molecular z axis. Intra- and inter-Kramers transitions are marked with blue and red data points, respectively. Powder EPR data are included in the low-field region; three components are observed at each frequency, corresponding to the three components of the effective Landé **g** tensor associated with the lowest Kramers doublet (see the legend). The solid lines represent the best simulation of the combined data sets (both single-crystal and powder measurements), employing eq 1 and the single set of Hamiltonian and parameters given in the main text. The thin gray line would be the expectation for the intra-Kramers transition in the absence of rhombic anisotropy (E = 0); the data clearly depart from this expectation, providing a constraint on the E parameter. Inset: Representative single-crystal EPR spectra for **1** collected at 1.3 K, demonstrating the observation of three ground-state resonances. Intra- and inter-Kramers transitions are marked with blue and red arrows, respectively.

field single-crystal data in Figure 2. Indeed, acceptable simulations can be obtained with both positive and negative D parameters (see Figure S5, Supporting Information). To discriminate between these two cases, low-field powder EPR measurements were performed (see Figure S6, Supporting Information); data points corresponding to the three components of the effective **g** tensor associated with the lowest Kramers doublet are included in the low-field portion of Figure 2. First, note that the highest field (lowest effective g) data points for the powder overlay exactly the single-crystal data, thus confirming that the field was well aligned with the hard axis for the high-field measurements. The thick solid curves in Figure 2 correspond to the best simulations of the combined data sets using eq 1, assuming a positive D value and a spin of $S = {}^3/_2$. The resulting parameters are D = +11 cm^{-1}, $|E|$ = 3.2 cm^{-1}, $g_x = g_y$ = 1.89, and g_z = 1.58. A reasonable simulation can be obtained for the negative D case as well. However, it yields g values greater than 2.00 (g_y = 2.50 and g_{av} = 2.13), whereas the principal Landé values must be less than 2.00 for an orbitally nondegenerate atom with less than a half-filled d shell, as is the case for octahedrally coordinated Re^{IV}, i.e., L = 0. In other words, the negative D (easy axis) simulation is physically unreasonable. We thus conclude that the D value is positive for **1**, and we shall see below that the situation is even more definitive in the case of compound **2**.

Returning to the discussion of the high-field single-crystal measurements, it is notable that the low-field intra-Kramers transitions in Figure 2 do not lie on a straight line that intersects the origin (thin gray line). This may be understood in terms of an avoided level crossing caused by the rhombic E term in eq 1, as illustrated in Figure 3. Moreover, this situation also explains the broadening of the intra-Kramers resonance

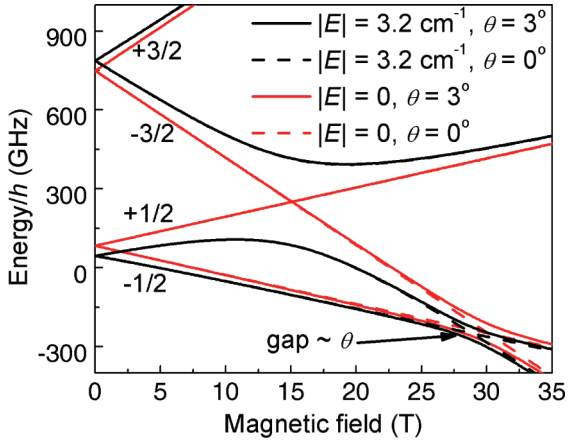

Figure 3. Zeeman diagram for compound **1** generated from eq 1 with D = +11 cm^{-1} and g_z = 1.58, considering different E values and field misalignment angles θ (see the legend), where θ = 0 corresponds to $B||z$. The approximate spin projection (M_S) of each state is labeled in the low-field region of the figure. The figure demonstrates that the avoided crossing at ~15 T is determined entirely by E while the one at ~28 T is determined solely by θ. Consequently, different regions of the data in Figure 2 constrain these two parameters.

with increasing frequency. In the absence of an E term, there would be no interaction between the $M_S = -{}^3/_2$ and $+{}^1/_2$ states, the spectrum would be linear in B_z (red curves in Figure 3), and the intra-Kramers data would lie on a straight line passing through the origin. Consequently, the departure of the low-field data from the gray line in Figure 2 provides one of the main constraints on E, the other being the splitting between the x and y components of the powder spectrum. Meanwhile, the inter-Kramers transitions above 15 T primarily constrain D and g_z. Finally, a small field misalignment was unavoidable due to the fact that a single-axis crystal rotation does not guarantee exact coincidence with the molecular z axis. This misalignment is solely responsible for the second avoided crossing (and the magnitude of the resultant gap; see Figure 3) at ~28 T, but it does not affect the low-field data significantly. Therefore, the deduced misalignment angle of θ = 3° was constrained very precisely from the 28 T minimum seen in the fit to the single-crystal data in Figure 2. Thus, even though the high-field simulation contains four variables (D, E, g_z, and θ), the obtained parameters are very well constrained. Moreover, they are further constrained by the powder measurements.

The E parameter obtained from the preceding analysis is quite substantial, corresponding to $|E/D|$ = 0.294, which is very close to the maximum allowable value of 1/3. For the extreme biaxial case in which $E = |D|/3$, the $D > 0$ and $D < 0$ parametrizations are in fact equivalent. It is precisely for this reason that good simulations can be obtained for both cases. In other words, the two parametrizations are similar (see Figure S5, Supporting Information), although it should be stressed that the powder measurements clearly favor the positive D scenario. Nevertheless, the underlying magnetic properties resulting from either biaxial parametrization would be expected to be quite similar.

Magnetometry and EPR Spectroscopy of 2 and 3. Due to the difficulty associated with interpreting EPR data from a dynamic chain system, where collective spin wave resonance is

dx.doi.org/10.1021/ja301338d | J. Am. Chem. Soc. 2012, 134, 7521−7529

observed instead of discrete paramagnetic resonance,[16] zero-field splitting parameters for Re^{IV} were not directly obtained from the EPR data for the chain compound **4**. As a means of isolating the magnetic contribution of the Re^{IV} ions within the chain, the isostructural compound **2** was prepared. Here, the paramagnetic Mn^{II} ions have been replaced by diamagnetic Zn^{II} ions to prevent significant exchange interactions involving the Re^{IV} centers while preserving any effects that stem from connection of $[ReCl_4(CN)_2]^{2-}$ units to other metal centers via the cyanide ligands. To confirm the magnetic isolation of the Re^{IV} centers, variable-temperature dc magnetic susceptibility data were collected for a microcrystalline sample of **2**. At 300 K, $\chi_M T$ = 1.30 $cm^3 \cdot K/mol$, a value that is expected for an $S = {}^3/_2$ spin center with g = 1.66. In addition, this g value is in good agreement with that previously obtained from magnetization data for **1** (g = 1.65).[4] For temperatures below 70 K, $\chi_M T$ starts to drop, continuing all the way to the minimum measurement temperature 1.8 K. Close inspection of the dc magnetic susceptibility data for **2** and **1** (see Figure S7, Supporting Information) reveals virtually identical behavior. Indeed, the $\chi_M T$ vs T plots of **1** and **2** are essentially superimposable, indicating an absence of inter- and/or intrachain magnetic interactions in **2**. As such, the downturn in $\chi_M T$ can be attributed to the magnetic anisotropy of the Re^{IV} center. Importantly, ac magnetic susceptibility measurements as a function of both frequency and temperature on a polycrystalline sample of **2** revealed no slow relaxation behavior at or above 1.8 K.

To further investigate the magnetic anisotropy in **2**, EPR measurements were carried out on a powder sample (see Figure 4). Analogous to the data obtained for compound **1**, three spectral features are resolved, corresponding to the principal components of the effective **g** tensor associated with the lowest Kramers doublet. In the case of easy-plane anisotropy ($D > 0$), the x and y components should occur at fields below the spin-only g = 2.00 position (dashed line) while the z component should occur above; the opposite would hold for the easy-axis ($D < 0$) case. As seen in Figure 4, the powder measurements clearly indicate easy-plane-type anisotropy with $D > 0$, although they do not permit a direct determination of the magnitude of D. Meanwhile, the sizable splitting between the x and y components of the spectrum again signifies appreciable biaxiality, corresponding to a significant E term. Attempts to detect inter-Kramers transitions were unsuccessful, as sufficiently sized single crystals have thus far not been obtainable. Therefore, for the purposes of simulation, we were forced to adopt the value of D = +11 cm^{-1} obtained for **1**. The solid curves in Figure 4 represent the best simulation of the peak positions employing eq 1 with $|E|$ = 2.1 cm^{-1}, $g_x = g_y$ = 1.78, and g_z = 1.94. As noted already, it is impossible to obtain any reasonable simulation with $D < 0$. However, the E value obtained is rather well constrained by the splitting between the x and y components of the powder spectrum. Therefore, these simulations unambiguously demonstrate that **2** possesses easy-plane-type anisotropy and appreciable transverse anisotropy, in analogy with **1**.

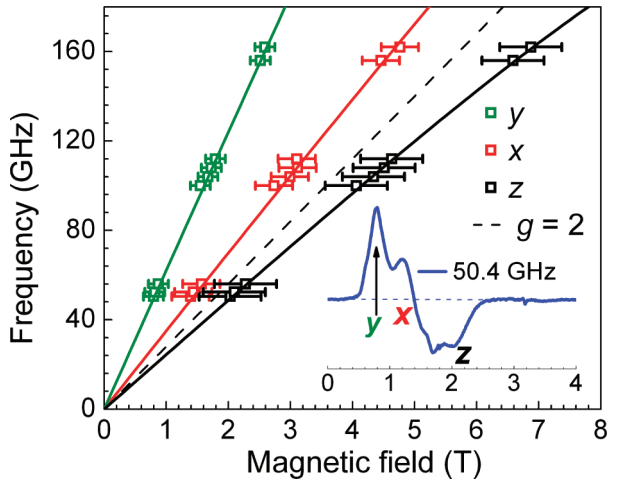

Figure 4. Frequency dependence of the EPR peak positions deduced from powder studies of compound **2** at 5 K. The inset shows a representative powder spectrum. Three resonance branches are observed, corresponding to the three principal components of the effective Landé **g** tensor associated with the lowest Kramers doublet (field parallel to x, y, and z). The solid lines are best simulations employing eq 1 and the parameters discussed in the main text. The dashed line represents the g = 2.00 position. The observation of one resonance above g = 2.00, and two below, is indicative of easy-plane-type anisotropy (see the main text for a further explanation).

To exclude the possibility that magnetic exchange coupling may act to invert the sign of D in the chain compound **4** relative to its constituent $[ReCl_4(CN)_2]^{2-}$ units, compound **3** was prepared and investigated. In particular, magnetic and EPR measurements were carried out on polycrystalline samples of **3** to study the zero-field splitting parameters of the Re^{IV} center in the presence of magnetic exchange coupling (see Figure S8, Supporting Information). First, the exchange coupling was probed through variable-temperature dc magnetic susceptibility measurements. At 300 K, $\chi_M T$ = 9.53 (cm^3 K)/mol, slightly lower than the calculated value of $\chi_M T$ = 10.62 (cm^3 K)/mol for an isolated Re^{IV} ($S = {}^3/_2$) center and two Mn^{II} ($S = {}^5/_2$) centers with g_{av} = 2.00. As the temperature is lowered, the value of $\chi_M T$ begins to drop, gradually at first and then abruptly below 70 K. This decrease with decreasing temperature indicates the presence of antiferromagnetic interactions between the Re^{IV} and Mn^{II} centers within the molecule. A fit to the data for **3**, employing the program MAGFIT 3.1[17] and the Hamiltonian $\hat{H} = -2J(\hat{S}_{Re} \cdot \hat{S}_{Mn1} + \hat{S}_{Re} \cdot \hat{S}_{Mn2})$, afforded J = −3.0(4) cm^{-1} and g = 1.98. These values are comparable to those of J = −5.4(4) cm^{-1} and g = 1.88 obtained for compound **4**. The slight difference in the magnitude of J may be due to the differences in the ligand field of Mn^{II} and the small variation in the Mn−N−C angles. Considering the very similar metal coordination environments in **3** and **4**, compound **3** should provide a reasonable model of the Mn···Re···Mn motif in **4**. Finally, we note that slow relaxation was not observed in the variable-frequency ac susceptibility measurements at temperatures above 1.8 K, even in the presence of an applied dc field.

EPR studies performed on **3** confirm that the Re^{IV} center possesses a positive D parameter, lending further weight to arguments that **4** also experiences easy-plane-type anisotropy. Figure 5 plots the frequency dependence of high-frequency EPR peak positions obtained from studies of a powder sample of **3** at 3.5 K, with the inset displaying a representative spectrum collected in first-derivative mode at 208 GHz. Three relatively strong features are observed, labeled as α_y, α_z, and β. At high fields and frequencies, the slopes of the α_y and α_z branches agree with expectations for standard EPR transitions with ΔM_S = 1 and $g \approx 2$. Meanwhile, the slope associated with the β branch suggests that it is a double quantum transition with ΔM_S = 2 and $g \approx 4$. We associate the α_y and α_z branches

dx.doi.org/10.1021/ja301338d | J. Am. Chem. Soc. 2012, 134, 7521−7529

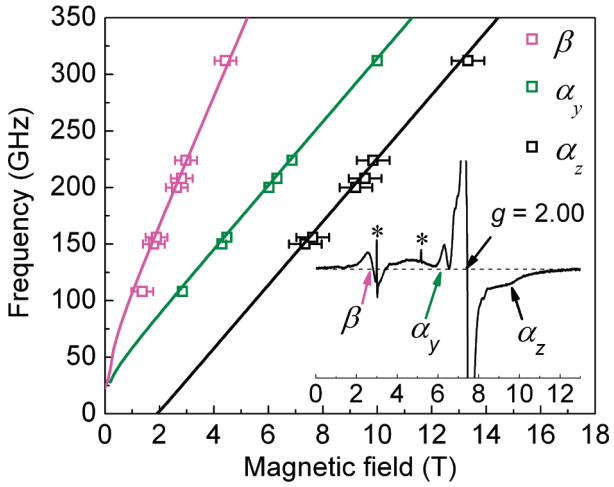

Figure 5. Frequency dependence of the EPR peak positions obtained from studies of a powder sample of **3** at 3.5 K. The solid lines are the best simulations employing eq 1 and the parameters discussed in the main text. The inset displays a representative spectrum collected in first-derivative mode at 208 GHz. The strong truncated feature at g = 2.00 is likely due to paramagnetic impurities and/or uncoupled Mn^{II} centers, while the sharp signals marked with asterisks are impurity signals from molecular oxygen absorbed in the sample holder. The broader anisotropic signals labeled α correspond to conventional ΔM_S = 1 transitions, while the β resonance corresponds to a double quantum transition (see the main text for a detailed explanation).

with the parallel (z) and perpendicular (y) extremes of the high-field spectrum. Note that the low-field spectrum would be rather more complex, thereby illustrating the importance of high-field measurements.

Unlike the powder results for compounds **1** and **2**, the α_y and α_z resonance branches correspond to excitations within a coupled molecular spin state experiencing zero-field splitting. It is for this reason that the high-field portions of the spectrum extrapolate to finite zero-field offsets, unlike the transitions within the lowest Kramers doublet in the case of **1** and **2**. Most importantly, the zero-field offsets deduced from Figure 5 provide direct information on the anisotropy associated with the $ReMn_2$ molecular units of **3**. The results may be interpreted by treating the molecule according to its approximate $S_{total} = S_{Mn1} + S_{Mn2} - S_{Re} = {}^5/_2 + {}^5/_2 - {}^3/_2 = {}^7/_2$ ground state that arises from antiferromagnetic coupling between Re^{IV} and Mn^{II} centers. The solid curves are the simulations obtained employing eq 1 and the molecular zero-field-splitting parameters D = +0.3 cm^{-1}, $|E|$ = 0.03 cm^{-1}, and g = 2.00, with $S = {}^7/_2$. As noted above, the α_z branch corresponds to the ground-state transition ($M_S \approx -{}^7/_2$ to $-{}^5/_2$) with the field being parallel to the molecular z axis, while α_y corresponds to the same transition but with the field parallel to y. The x component is buried within the very large signal close to g = 2.00. The simulations also successfully account for the double quantum transition (β, or $M_S \approx -{}^7/_2$ to $-{}^3/_2$), assuming that it belongs to the y component of the spectrum. It is noteworthy that double quantum transitions usually appear when the field is applied perpendicular to the dominant quantization axis (z axis), which is consistent with our observations and provides further confirmation for the peak assignments.

Although fine structure peaks are not resolved, observation of the y and z extremes provide a very robust constraint on the sign of the D parameter. Indeed, the fact that the shift of the z component to the high-field side of the isotropic g = 2.00 position is substantially greater than that of the y component to the low-field side can be taken as unambiguous evidence that the molecular anisotropy is of the easy-plane type, i.e., $D > 0$. One could question the validity of the preceding analysis for a molecule in which the exchange coupling is weak in comparison to the anisotropy ($J < D$). However, extensive studies on other simple trinuclear and tetranuclear molecules in this same $J < D$ regime have shown that EPR spectra essentially retain the characteristics of a giant spin, particularly at the low- and high-field extremes that dominate at low temperatures, i.e., the same regions of the powder spectrum that we focus on here.[18]

We can make a rough estimate of the anisotropy parameters associated with the Re^{IV} center using the projection method.[19] The zero-field splitting associated with octahedrally coordinated high-spin Mn^{II} may be assumed to be negligible,[20] such that the anisotropy of **3** will be dominated by Re^{IV}. The projection method then gives $\vec{D}_{mol} = 0.0143 \times \vec{D}_{Re}$, where $\vec{D}_{mol}$ and $\vec{D}_{Re}$ are the anisotropy tensors of the $ReMn_2$ molecule and the Re^{IV} center, respectively. We thus estimate that $D_{Re} \approx +21$ cm^{-1} and $E_{Re} \approx 2.1$ cm^{-1}. However, due to the significant uncertainty associated with the resonance positions in Figure 5 and the many simplifying assumptions made in the analysis, these values should be considered as only approximate. Nevertheless, the data once again confirm a positive D parameter with considerable rhombicity.

Discussion of the Magnetic Relaxation Process. High-spin Mn^{II} complexes typically possess nearly negligible magnetic anisotropy.[20] As such, the magnetic relaxation barrier in **4** must arise primarily from the anisotropy of the Re^{IV} centers. However, the EPR studies reported here clearly indicate the presence of a positive D for Re^{IV}. Moreover, the theoretical anisotropy relaxation barriers of Δ_A = 25 and 32 cm^{-1} for **4** obtained using the magnitude of D (assuming D is negative) deduced both by EPR and magnetic measurements, respectively, are in stark disagreement with the experimental barrier of 12 cm^{-1}. These curious factors suggest that new physics may be at play in governing the magnetic relaxation of **4**.

If one considers the doubly degenerate $M_S = \pm{}^1/_2$ ground levels of an isolated $S = {}^3/_2$ molecule with positive D, then extreme quantum tunneling effects prevent localization of the molecular magnetic moment within the xy plane, i.e., $\langle \hat{S}_x \rangle = \langle \hat{S}_y \rangle = 0$. However, the coupling of such spins, one-by-one, to form a ferrimagnetic chain, results in a gradual suppression of these tunneling effects. In such a description, the chain possesses a giant spin, S, which scales with the chain correlation length, l_z. In the case of **4**, the coordination environments of the Re^{IV} centers are collinear throughout the chains, with the z direction parallel to the direction of chain propagation. As such, the preferred orientation of the giant spin, S, lies in the plane perpendicular to the chain (see Figure 6). A transverse anisotropy then creates a preferred axis within this plane, although quantum tunneling may still prevent localization of S for small chain lengths. However, as the chain correlation length grows, these fluctuations diminish as the quantum tunneling is increasingly suppressed. In fact, the relaxation time due to tunneling, τ_0, should increase exponentially with increasing chain length. One method of visualizing such an effect is to consider the probability that all spins within the chain tunnel simultaneously, as would be required if the total spin were to tunnel coherently. Clearly, this probability decreases exponentially with increasing number of spins in

dx.doi.org/10.1021/ja301338d | J. Am. Chem. Soc. 2012, 134, 7521−7529

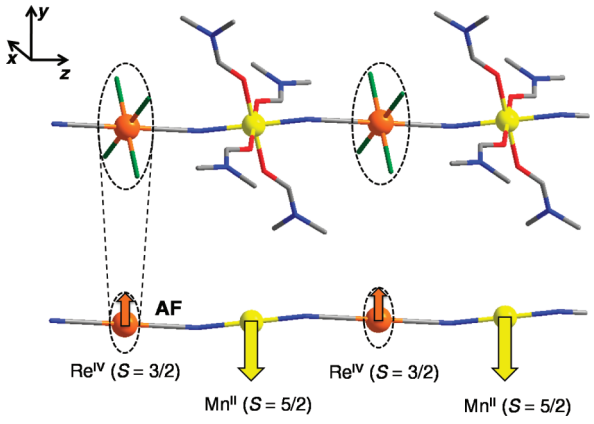

Figure 6. Structure (upper) and spin arrangement (lower) of chain compound **4**. The atoms are colored as follows: Re^{IV} = orange, Mn^{II} = yellow, Cl = green, N = blue, and C = gray. The black dashed circles denote the local *xy* plane of each Re^{IV} center, which is determined by the four coplanar chlorine atoms; the *z* axis is parallel to the chain direction. In the classical ground state, the Mn^{II} spins (yellow arrows) are locked into an antiparallel arrangement relative to the Re^{IV} spins (orange arrows); the easy-plane anisotropy associated with the Re^{IV} centers then constrains the spins within the *xy* plane on both sublattices.

the chain. Consequently, in the limit of large correlation length, *S* can be treated classically.

Figure 7 depicts the classical potential energy surface in spin space corresponding to the zero-field operator equivalent terms

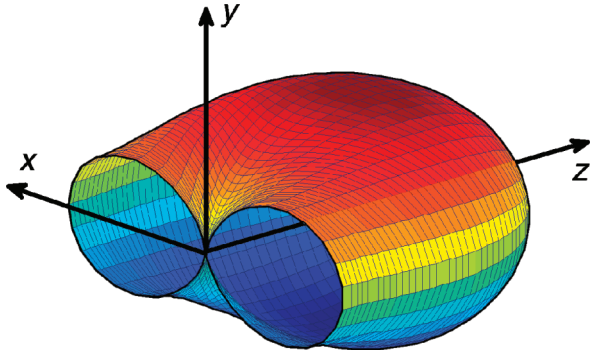

Figure 7. Classical magnetoanisotropy energy surface corresponding to the zero-field operator equivalent terms given in eq 1, with $D > 0$ and $|E|/|D|$ equal to the ratio found from the present EPR experiments on compound **2**. The radial distance to the surface represents the energy of a spin as a function of its orientation; zero energy has been chosen to correspond to the case when the spin is parallel to *y*, and only the $z > 0$ surface is shown to aid viewing of the cross-section in the *xy* plane. As can be seen, the spin experiences an anisotropic kinetic barrier against reversal from $+y$ to $-y$, with the barrier minimum occurring along $\pm x$.

given in eq 1, with $D > 0$ and $|E/D|$ equal to the ratio found from the present EPR experiments. The radial distance to the surface represents the energy of a spin as a function of its orientation. The minimum energy occurs when the spin points along $\pm y$, with an energy barrier separating these two orientations. The barrier maximum occurs in the *yz* plane and is determined by *D*. Meanwhile, it is *E* that sets the energy scale of the barrier minimum for rotation in the *xy* plane. In the large l_ξ limit, the anisotropy barrier against coherent rotation of an entire chain will be quite considerable, because the anisotropies of the individual Re^{IV} centers sum together. Nevertheless, we propose that magnetization dynamics can still proceed via the usual Glauber mechanism,[5] except that the relevant anisotropy energy scale is determined by *E* rather than *D*. As such, the anisotropy energy associated with the reversal of a single Re^{IV} spin within the chain is given by $\Delta_A = 2|E|S^2$. Considering the value of $|E| = 2.1\ cm^{-1}$ deduced from the EPR measurements on **2**, the anisotropy energy of **4** can be estimated at $\Delta_A = 9.5\ cm^{-1}$. Using the previously obtained value of the correlation energy of $\Delta_\xi = 19\ cm^{-1}$ along with the expression for the overall relaxation barrier for a chain in the finite-size limit $\Delta_\tau = \Delta_A + \Delta_\xi$, a value of $\Delta_\tau = 29\ cm^{-1}$ is obtained for **4**. Remarkably, this value is in excellent agreement with the experimentally determined value of $\Delta_\tau = 31\ cm^{-1}$, which has heretofore been unexplainable in terms of magnetic anisotropy and correlation. Moreover, in our previous work on the isostructural chain compounds $(DMF)_4MReCl_4(CN)_2$ (M = Mn, Fe, Co, Ni), the experimental correlation energy of $(DMF)_4NiReCl_4(CN)_2$ was found to be $\Delta_\xi = 8.8\ cm^{-1}$. Taking the small contribution of the zero-field splitting of octahedral Ni^{II} ions and the anisotropy barrier ($\Delta_A = 9.5\ cm^{-1}$) estimated from EPR data into account, the overall relaxation barrier $\Delta_\tau = \Delta_A + \Delta_\xi = 18.3\ cm^{-1}$ agrees very well with the experimental value of $\Delta_\tau = 20\ cm^{-1}$, giving further evidence for the relaxation process via transverse anisotropy. Finally, note that the anisotropy energies of the CoRe and FeRe chain compounds are different, as the important contribution of zero-field splitting from high-spin Co^{II} and Fe^{II} enables a more complicated relaxation mechanism.

A small number of previous studies have uncovered the presence of slow magnetic relaxation in single-molecule and single-chain magnets with $D > 0$. For instance, a mixed-valence alternating high-spin Fe^{II}, low-spin Fe^{III} chain compound was shown to exhibit slow magnetization reversal with easy-plane anisotropy.[21] Here, the authors attributed the relaxation behavior to a mutually orthogonal arrangement of the Fe^{II} molecular axes, which serves to induce Ising interactions along the chain. In another instance, a trinuclear Cu_3 single-molecule magnet was reported to display easy-plane anisotropy, with $U_{eff} = 5\ cm^{-1}$.[22] In this work, the authors pointed out that the relaxation follows an Orbach process involving the exchange-coupled excited states of the cluster. Similarly, we recently reported the observation of slow magnetic relaxation in a pseudotetrahedral Co^{II} complex with easy-plane anisotropy.[23] For the reported molecule, a field-induced bottleneck of the direct relaxation between the $M_S = \pm{}^1/_2$ levels generated Orbach relaxation pathways through the excited $M_S = {}^3/_2$ levels. Finally, a Fe_3Cr cluster that features constituent Cr^{III} and Fe^{III} centers with hard-axis anisotropy was shown to display single-molecule magnet behavior.[24] This phenomenon was attributed to an overall molecular easy-axis anisotropy that stems from the presence of peripheral hard-axis-type Fe^{III} centers, whose anisotropy tensors align orthogonal to the 3-fold molecular axis. Note that, in all of these cases, the barrier to spin relaxation is still a consequence of *D*, albeit positive in sign. As such, to our knowledge, **4** represents the first example of a compound in which slow magnetic relaxation arises due to *E*.

■ CONCLUSIONS AND OUTLOOK

The foregoing results demonstrate that slow magnetic relaxation in coordination compounds can arise from transverse anisotropy. In particular, high-field, high-frequency EPR measurements on a series of model compounds show that

dx.doi.org/10.1021/ja301338d | J. Am. Chem. Soc. 2012, 134, 7521−7529

the magnetic relaxation in the single-chain magnet $(DMF)_4MnReCl_4(CN)_2$ is governed by a nonzero E term, despite the presence of a positive D. Furthermore, the anisotropy energy of the compound can be expressed as $\Delta_A = 2|E|S^2$ to give a value of $\Delta_A = 9.8\ cm^{-1}$. The overall relaxation barrier can then be expressed as $\Delta_\tau = \Delta_A + \Delta_\xi$ to give a value of $\Delta_\tau = 29\ cm^{-1}$. Remarkably, this value is in excellent agreement with the experimentally determined value of $\Delta_\tau = 31\ cm^{-1}$. The observation of slow relaxation arising from E is, to our knowledge, an unprecedented phenomenon in molecular magnetism, and it represents a potentially new design strategy toward constructing low-dimensional magnetic materials. Future work will focus on further understanding the effects of large transverse anisotropy on related compounds, in particular molecular systems where quantum tunneling of the magnetization is still a significant contributor to overall magnetic relaxation. In addition, work is under way to design new molecular building units that feature large positive D and significant E to direct the formation of new single-chain magnets with high relaxation barriers.

■ ASSOCIATED CONTENT

Supporting Information

Table and CIF files giving crystallographic data and figures giving additional data. This material is available free of charge via the Internet at http://pubs.acs.org.

■ AUTHOR INFORMATION

Corresponding Author

shill@magnet.fsu.edu; jrlong@berkeley.edu

Author Contributions

‖These authors contributed equally to this work.

Notes

The authors declare no competing financial interest.

■ ACKNOWLEDGMENTS

This research was funded by Department of Energy/Lawrence Berkeley National Laboratory Grant 403801 (synthesis) and National Science Foundation (NSF) Grants CHE-1111900 (magnetism) and DMR-0804408 (EPR). A portion of the work was performed at the National High Magnetic Field Laboratory, which is supported by the NSF (Grant DMR-0654118) and the State of Florida. We thank Tyco Electronics for providing T.D.H. with a graduate fellowship, Prof. R. Clérac for helpful discussions, and Mr. J. M. Zadrozny for experimental assistance.

■ REFERENCES

(1) (a) Sessoli, R.; Tsai, H. L.; Schake, A. R.; Wang, S.; Vincent, J. B.; Folting, K.; Gatteschi, D.; Christou, G.; Hendrickson, D. N. *J. Am. Chem. Soc.* **1993**, *115*, 1804. (b) Sessoli, R.; Gatteschi, D.; Caneschi, A.; Novak, M. A. *Nature* **1993**, *365*, 141. (c) Gatteschi, D.; Sessoli, R.; Villain, J. *Molecular Nanomagnets*; Oxford University Press: New York, 2006; see also references therein. (d) Milios, C. J.; Vinslava, A.; Wernsdorfer, W.; Moggach, S.; Parsons, S.; Perlepes, S. P.; Christou, G.; Brechin, E. K. *J. Am. Chem. Soc.* **2007**, *129*, 2754. (e) Freedman, D. E.; Jenkins, D. M.; Iavarone, A. T.; Long, J. R. *J. Am. Chem. Soc.* **2008**, *130*, 2884. (f) Yoshihara, D.; Karasawa, S.; Koga, N. *J. Am. Chem. Soc.* **2008**, *130*, 10460. (g) Freedman, D. E.; Harman, W. H.; Harris, T. D.; Long, G. J.; Chang, C. J.; Long, J. R. *J. Am. Chem. Soc.* **2010**, *132*, 1224. (h) Zhang, Y. Z.; Wang, B. W.; Sato, O.; Gao, S. *Chem. Commun.* **2010**, *46*, 6959. (i) Harman, W. H.; Harris, T. D.; Freedman, D. E.; Fong, H.; Chang, A.; Rinehart, J. D.; Ozarowski, A.; Sougrati, M. T.; Grandjean, F.; Long, G. J.; Long, J. R. *J. Am. Chem. Soc.* **2010**, *132*, 18115. (j) Zadrozny, J. M.; Freedman, D. E.; Jenkins, D. M.; Harris, T. D.; Iavarone, A. T.; Mathoniere, C.; Clérac, R.; Long, J. R. *Inorg. Chem.* **2010**, *49*, 8886. (k) Pedersen, K. S.; Dreiser, J.; Nehrkorn, J.; Gysler, M.; Schau-Magnussen, M.; Schnegg, A.; Holldack, K.; Robert, B.; Stergios, P.; Weihe, H.; Tregenna-Piggott, P.; Waldmann, Oliver.; Bendix, J. *Chem. Commun.* **2011**, *47*, 6918. (l) Das, A.; Gieb, K.; Krupskaya, Y.; Demeshko, S.; Sebastian, D.; Klingeler, R.; Kataev, V.; Buchner, B.; Muller, P.; Meyer, F. *J. Am. Chem. Soc.* **2011**, *133*, 3433. (m) Rinehart, J. D.; Fang, M.; Evans, W. J.; Long, J. R. *Nat. Chem.* **2011**, *3*, 538. (n) Rinehart, J. D.; Fang, M.; Evans, W. J.; Long, J. R. *J. Am. Chem. Soc.* **2011**, *133*, 14236. (o) Zadrozny, J. M.; Long, J. R. *J. Am. Chem. Soc.* **2011**, *133*, 20732.

(2) (a) Garanin, D. A.; Chudnovsky, E. M. *Phys. Rev. B* **1997**, *56*, 11102. (b) Leuenberger, M. N.; Loss, D. *Nature* **2001**, *410*, 789. (c) Jo, M.-H.; Grose, J. E.; Liang, W.; Baheti, K.; Deshmukh, M. M.; Sokol, J. J.; Rumberger, E. M.; Hendrickson, D. N.; Long, J. R.; Park, H.; Ralph, D. C. *Nano Lett.* **2006**, *6*, 2014. (d) Ardavan, A.; Rival, O.; Morton, J. J. L.; Blundell, S. J.; Tyryshkin, A. M.; Timco, G. A.; Winpenny, R. E. P. *Phys. Rev. Lett.* **2007**, *98*, 57201. (e) Bogani, L.; Wernsdorfer, W. *Nat. Mater.* **2008**, *7*, 179. (f) Stamp, P. C. E.; Gaita-Arino, A. *J. Mater. Chem.* **2009**, *19*, 1718. (g) Loth, S.; von Bergmann, K.; Ternes, M.; Otte, A. F.; Lutz, C. P.; Heinrich, A. J. *Nat. Phys.* **2010**, *6*, 340.

(3) (a) Caneschi, A.; Gatteschi, D.; Lalioti, N.; Sangregorio, C.; Sessoli, R.; Venturi, G.; Vindigni, A.; Rettori, A.; Pini, M. G.; Novak, M. A. *Angew. Chem., Int. Ed.* **2001**, *40*, 1760. (b) Clérac, R.; Miyasaka, H.; Yamashita, M.; Coulon, C. *J. Am. Chem. Soc.* **2002**, *124*, 12837. (c) Lescouëzec, R.; Vaissermann, J.; Ruiz-Pérez, C.; Lloret, F.; Carrasco, R.; Julve, M.; Verdaguer, M.; Dromzée, Y.; Gatteschi, D.; Wernsdorfer, W. *Angew. Chem., Int. Ed.* **2003**, *42*, 1483. (d) Liu, T. F.; Fu, D.; Gao, S.; Zhang, Y. Z.; Sun, H. L.; Su, G.; Liu, Y. J. *J. Am. Chem. Soc.* **2003**, *125*, 13976. (e) Wang, S.; Zuo, J.-L.; Gao, S.; Song, Y.; Zhou, H.-C.; Zhang, Y.-Z.; You, X.-Z. *J. Am. Chem. Soc.* **2004**, *126*, 8900. (f) Ferbinteanu, M.; Miyasaka, H.; Wernsdorfer, W.; Nakata, K.; Sugiura, K.; Yamashita, M.; Coulon, C.; Clérac, R. *J. Am. Chem. Soc.* **2005**, *127*, 3090. (g) Coulon, C.; Miyasaka, H.; Clérac, R. *Struct. Bonding (Berlin)* **2006**, *122*, 163. (h) Bernot, K.; Bogani, L.; Caneschi, A.; Gatteschi, D.; Sessoli, R. *J. Am. Chem. Soc.* **2006**, *128*, 7947. (i) Miyasaka, H.; Madanbashi, T.; Sugimoto, K.; Nakazawa, Y.; Wernsdorfer, W.; Sugiura, K.; Yamashita, M.; Coulon, C.; Clérac, R. *Chem.—Eur. J* **2006**, *12*, 7028. (j) Miyasaka, H.; Julve, M.; Yamashita, M.; Clérac, R. *Inorg. Chem.* **2009**, *48*, 3420 and references therein. (k) Feng, X.; Harris, T. D.; Long, J. R. *Chem. Sci.* **2011**, *2*, 1688−1694. (l) Yoon, J. H.; Lee, J. W.; Won, R. D.; Choi, S. Y.; Yoon, S. W.; Suh, B. J.; Koh, E. K.; Kim, H. C.; Hong, C. S. *Inorg. Chem.* **2011**, *50*, 11306. (m) Escuer, A.; Vlahopoulout, G.; Mautner, F. A. *Inorg. Chem.* **2011**, *50*, 2717. (n) Ding, M.; Wang, B.; Wang, Z.; Zhang, J.; Fuhr, O.; Fenske, D.; Gao, S. *Chem.—Eur. J.* **2012**, *18*, 915.

(4) Harris, T. D.; Bennett, M. V.; Clérac, R.; Long, J. R. *J. Am. Chem. Soc.* **2010**, *132*, 3980.

(5) Glauber, R. J. *J. Math. Phys.* **1963**, *4*, 294.

(6) (a) Suzuki, M.; Kubo, R. *J. Phys. Soc. Jpn.* **1968**, *24*, 51. (b) Coulon, C.; Clérac, R.; Lecren, L.; Wernsdorfer, W.; Miyasaka, H. *Phys. Rev. B* **2004**, *69*, 132408.

(7) (a) Caneschi, A.; Gatteschi, D.; Sessoli, R.; Barra, A. L.; Brunel, L. C.; Guillot. *J. Am. Chem. Soc.* **1991**, *113*, 5873−5874. (b) Barra, A. L.; Gatteschi, D.; Sessoli, R. *Phys. Rev. B* **1997**, *56*, 8192. (c) Hill, S.; Edwards, R. S.; Aliaga-Alcalde, N.; Christou, G. *Science* **2003**, *302*, 1015−1018. (d) Inglis, R.; Jones, L. F.; Milios, C. J.; Datta, S.; Collins, A.; Parsons, S.; Wernsdorfer, W.; Hill, S.; Perlepes, S. P.; Piligkos, S.; Brechin, E. K. *Dalton Trans.* **2009**, 3403−3412.

(8) Yang, E.-C.; Kirman, C.; Lawrence, J.; Zakharov, L. N.; Rheingold, A. L.; Hill, S.; Hendrickson, D. N. *Inorg. Chem.* **2005**, *44*, 3827.

(9) *SMART Software Users Guide*, version 5.1; Bruker Analytical X-Ray Systems: Madison, WI, 1999.

(10) *APEX2*, version 2009; Bruker Analytical X-Ray Systems: Madison, WI, 1999.

(11) *SAINT Software Users Guide*, version 7.0; Bruker Analytical X-Ray Systems: Madison, WI, 1999.
(12) Sheldrick, G. M. *SADABS*, version 2.03; Bruker Analytical X-Ray Systems, Madison, WI, 2000.
(13) Sheldrick, G. M. *SHELXTL*, version 6.12; Bruker Analytical X-Ray Systems, Madison, WI, 2000.
(14) Takahashi, S.; Hill, S. *Rev. Sci. Instrum.* **2005**, *76* (2), 023114–10.
(15) (a) Park, K.; Novotny, M. A.; Dalal, N. S.; Hill, S.; Rikvold, P. A. *Phys. Rev. B* **2001**, *65* (1), 014426. (b) Hill, S.; Maccagnano, S.; Park, K.; Achey, R. M.; North, J. M.; Dalal, N. S. *Phys. Rev. B* **2002**, *65* (22), 224410.
(16) Oshima, Y.; Nojiri, H.; Asakura, K.; Sakai, T.; Yamashita, M.; Miyasaka, H. *Phys. Rev. B* **2006**, *73* (21), 214435.
(17) Schmitt, E. A. Ph.D. Thesis, University of Illinois at Urbana-Champaign, 1995.
(18) (a) Hill, S.; Datta, S.; Liu, J.; Inglis, R.; Milios, C. J.; Feng, P. L.; Henderson, J. J.; del Barco, E.; Brechin, E. K.; Hendrickson, D. N. *Dalton Trans.* **2010**, *39*, 4693. (b) Quddusi, H. M.; Liu, J.; Singh, S.; Heroux, K. J.; del Barco, E.; Hill, S.; Hendrickson, D. N. *Phys. Rev. Lett.* **2011**, *106*, 227201. (c) Heroux, K. J.; Quddusi, H. M.; Liu, J.; O'Brien, J. R.; Nakano, M.; del Barco, E.; Hill, S.; Hendrickson, D. H. *Inorg. Chem.* **2011**, *50*, 7367.
(19) *Electron Paramagnetic Resonance of Exchange Coupled Clusters*; Bencini, A., Gatteschi, D., Eds.; Springer: Berlin, 1990.
(20) Krzystek, J.; Ozarowski, A.; Telser, J. *Coord. Chem. Rev.* **2006**, *250* (17–18), 2308.
(21) Kajiwara, T.; Nakano, M.; Kaneko, Y.; Takaishi, S.; Ito, T.; Yamashita, M.; Igashira-Kamiyama, A.; Nojiri, H.; Ono, Y.; Kojima, N. *J. Am. Chem. Soc* . **2005**, *127*, 10150.
(22) Sanakis, Y.; Pissas, M.; Krzystek, J.; Telser, J.; Raptis, R. G. *Chem. Phys. Lett.* **2010**, *493*, 185.
(23) Zadrozny, J. M.; Liu, J.; Piro, N. A.; Chang, C. J.; Hill, S.; Long, J. R. *Chem. Commun.* **2012**, *48*, 3927.
(24) Tancini, E.; Rodriguez-Douton, M. J.; Sorace, L.; Barra, A.-L.; Sessoli, R.; Cornia, A. *Chem.—Eur. J* **2010**, *16*, 10482.